PROCEEDINGS OF SPIE

SPIEDigitalLibrary.org/conference-proceedings-of-spie

Satellite monitoring of sea ice dynamics at local scale

Michał Krupiński, Edyta Woźniak, Marek Ruciński, Wlodek Kofman, Anna Wawrzaszek, et al.

Michał Krupiński, Edyta Woźniak, Marek Ruciński, Wlodek Kofman, Anna Wawrzaszek, Alice Baronetti, Gianna Vivaldo, Antonello Provenzale, Mariasilvia Giamberini, "Satellite monitoring of sea ice dynamics at local scale," Proc. SPIE 12734, Earth Resources and Environmental Remote Sensing/GIS Applications XIV, 127341I (19 October 2023); doi: 10.1117/12.2684340

SPIE.

Event: SPIE Remote Sensing, 2023, Amsterdam, Netherlands

Satellite monitoring of sea ice dynamics at local scale

Michał Krupiński*[a], Edyta Woźniak[a], Marek Ruciński[a], Wlodek Kofman[a], Anna Wawrzaszek[a], Alice Baronetti[b], Gianna Vivaldo[b], Antonello Provenzale[b], Mariasilvia Giamberini[b]

[a]Centrum Badań Kosmicznych PAN, ul. Bartycka 18A, 00-716 Warszawa, Poland
[b] Istituto di Geoscienze e Georisorse del CNR, via G. Moruzzi 1, 56124 Pisa, Italy

ABSTRACT

Svalbard (Norway) is a "hotspot" of climate change. There, various research activities are taking place, most of them located at the Ny-Ålesund Research Station, on the shore of the Kingsfiord, mainly focused on understanding climate change dynamics and its effects on the Arctic marine and terrestrial ecosystems, including their interconnections. In fact, the fiord is a unique environment where the atmosphere, sea, land and their ecosystems are strictly connected. Among the other ones, Ny Ålesund hosts the Italian Arctic Station "Dirigibile Italia", a multidisciplinary research facility owned by the National Research Council of Italy (CNR), since 1997.

Currently, several scientific projects are developed at the Italian Station, dealing with physics and chemistry of the atmosphere and snow, microbial ecology and evolution, nutrients and ecosystems, biogeochemistry and energy fluxes, clouds, aerosols, gases and remote sensing.

One of the important parameters that influences the fiord dynamic is the sea ice occurrence. Sea ice in the fiord can form overnight due to strong wind and disappear as fast. Among other, it is expected that sea ice cover influences the air-sea gas exchange. Various sea ice remote sensing products are available from satellite data. However, they are generalised and do not provide high resolution daily maps. This means that fast ice formation and disappearance is not properly detected and available products are not detailed enough for local scale analysis.

In the literature, the analysis of available sea ice products has been performed to evaluate its usefulness for the local scale applications. Various limitations have been identified, including: generalization of sea ice extent, gaps in temporal coverage (e.g., some products are not generated on weekends), mismatches on sea ice extent between different products.

To overcome these limitations, usability of Sentinel-1 based products were considered within this study. Ice cover maps from Sentinel-1 data were generated using machine learning algorithms and various feature sets (e.g., GLCM, Hölder exponents). The goal of this algorithm is to develop detailed (with high spatial and temporal resolution) sea ice maps of the Kingsfiord.

Keywords: sea ice, detection, classification, Sentinel-1, Copernicus, Svalbard, remote sensing

1. INTRODUCTION

Sea ice is a key indicator of climate variability and change. Its extent is one of the Essential Climate Variables. It influences sea surface waves, air-sea exchange of moisture and gases and, most important, heat. Complex temporal and spatial sea ice measurements became possible since remote sensing satellites started to deliver the images from each part of the Earth [1].

Satellite sea ice monitoring covers the period of 45 years now, as the first sea ice products were produced for 1978 year. Currently, with increasing number of satellites, new products are developed and shared as the open data. Various products characteristics depend mostly on satellite sensor properties used for sea ice mapping. In Table 1, number of satellite products with daily temporal resolution have been listed. Despite high number of available products, they have some limitations. For example, the Norwegian Ice Service ice charts are generated only for week days. Moreover, only some of them provide the data up to present day. The pixel size of these products varies from 1 to 25 km. The list contains only the products which cover arctic regions, as our area of interest is located in the north of the Arctic Circle.

*mkrupinski@cbk.waw.pl; phone + 48 22 496 62 05; zoz.cbk.waw.pl

Earth Resources and Environmental Remote Sensing/GIS Applications XIV, edited by Karsten Schulz,
Ulrich Michel, Konstantinos G. Nikolakopoulos, Proc. of SPIE Vol. 12734, 127341I

· doi: 10.1117/12.2684340

1.1 Available ice extent products and their limitations

There are number of existing geospatial databases providing the information about the sea ice extent. Most of them are created by satellite image analysis. Table 1 contains the main characteristics of these databases and in Figure 1 examples of three product, generated for the same date are presented. Additionally, the Sentinel-1 image, acquired at the same date, is added to present the high level of details which can be observed. In the middle of red circle, Ny-Ålesund Research Station is located. By visual comparison of different products, it is possible to observe the main differences between them. For example, ASMR-2 product (Figure 1 b) is generated from pixels of various sizes, with many areas with no data about sea ice available (grey colour). Two other examples represent vector data, where the edge between sea and water is more detailed. Both of them seem to overestimate the area of sea covered by ice in comparison to Sentinel-1 image.

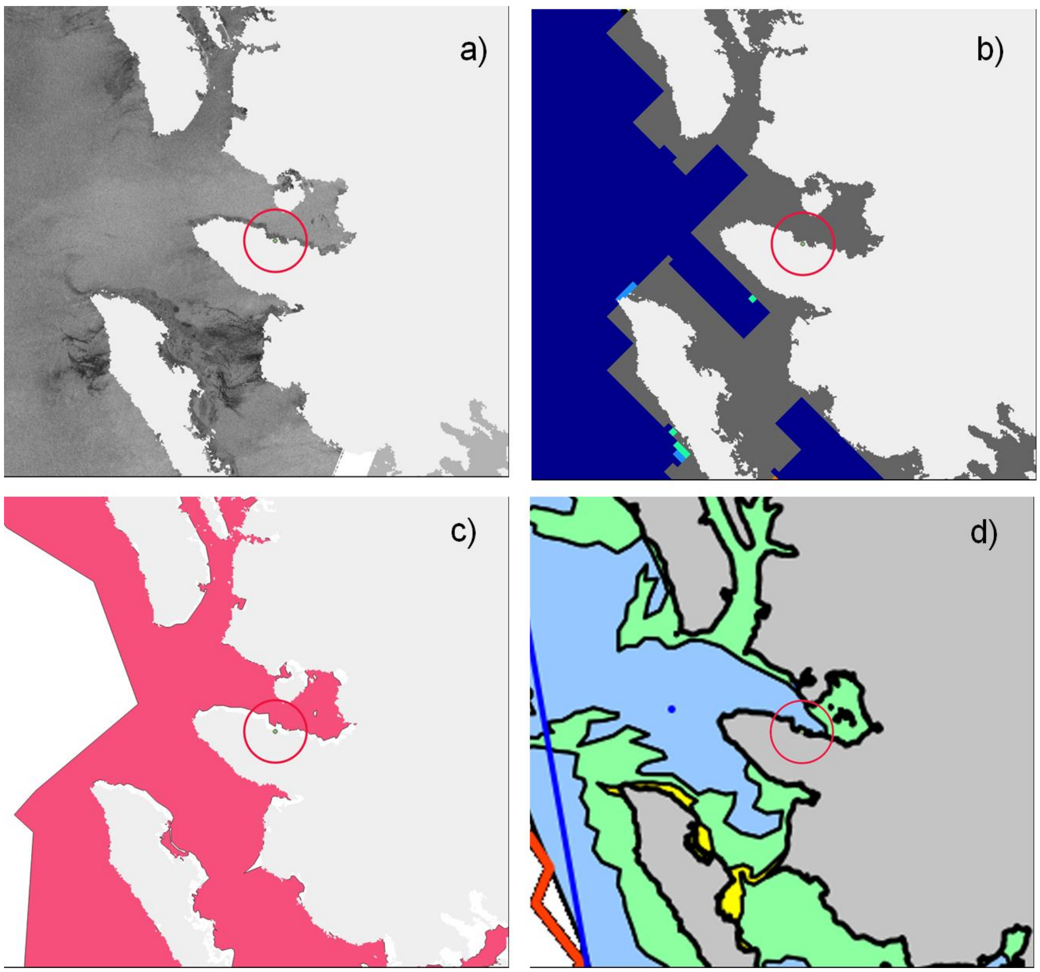

Figure 1. Sea ice extent on December 5th, 2019: a) Sentinel-1 satellite image (dark grey and black: ice, grey: water), b) ASMR-2 (navy blue: water, light blue and green: sea-ice, grey: no data), c) MIZ (red: sea-ice), d) Ice chart (light blue: water, green and yellow: sea-ice). Red circle – Ny-Ålesund Research Station area.

The analysed existing databases provide very valuable source of data for global and regional sea ice monitoring. At the same time, there are few reasons why they are not sufficient for local scale monitoring:

- low spatial resolution;
- non consistent temporal coverage;
- incoherent thematic information between the products.

Table 1. Basic characteristics of existing daily ice extent products.

Product	Spatial resolution	Temporal coverage	Sensors
Sea Ice Concentrations from Nimbus-7 SMMR and DMSP SSM/I-SSMIS Passive Microwave Data, Version 2 [2]	25 km	26/10/1978 to 31/12/2022	SMMR, SSM/I, SSMIS
Near-Real-Time DMSP SSMIS Daily Polar Gridded Sea Ice Concentrations, Version 2 [3]	25 km	1/11/2021 to present	SSMIS
NSIDC Sea Ice Index [2]	25 km	26/10/1978 to present	SMMR, SSM/I, SSMIS
AMSR-E sea ice concentration [4]	6.25 km	1/6/2002 to 4/10/2011	AMSR-E
AMSR2 sea ice concentration [4]	6.25 km	01/07/2012 to 17/11/2018	AMSR2
MODIS-AMSR2 sea-ice concentration [5]	1 km	27/08/2019 to present	MODIS, AMSR2
NSIDC Marginal Ice Zone (MIZ) Products, Version 1 [6]	N/A	19/102004 to present	Multiple sensors
Norwegian Ice Service Charts [7]	N/A	- to present	e.g., Sentinel-1, Radarsat-2

1.2 Proposed solution

In the scope of this paper, we develop a prototype of the daily product, with pixel size smaller than 100 m, for the area of Svalbard. We have used the state of the art, machine learning classification algorithms and tested various scenarios, where different feature sets were used.

2. METHODOLOGY

2.1 Data

Sentinel-1 satellites, as part of European Copernicus programme, provide open and unlimited access to data gathered almost continuously. Onboard of Sentinel-1 satellites, C-band synthetic aperture radar (SAR) instrument is operating in dual polarization (VV and VH), in one of four acquisition modes. Within this study, Level-1 Ground Range Detected (GRD) product of Extra-Wide swath (EW) mode was used. In this mode, the products are generated from 5 sub-swaths. The pixel size of analysed images was 8×40 m.

2.1 Study area

Figure 2. Map with Ny-Ålesund Research Station location.

Svalbard (Norway), located in the High Arctic, are a “hotspot” of climate change. The research conducted at the international Ny-Ålesund Research Station, on the shore of the Kingsfiord, is mainly focused on understanding climate change dynamics and its effects on the Arctic marine and terrestrial ecosystems, including their interconnections.

4.1 Experiment workflow

Proposed experiment is composed of five main steps (Figure 3). First, for one selected Sentinel-1 image, the reference dataset was created by visual interpretation of randomly selected points. It contains 250 points representing two classes – ice and water. Sentinel-1image was pre-processed by application of denoising algorithm [8] and Lee-Sigma filter. Denoising procedure mitigates the effect of pixel values differences between bursts of single image. This effect is mostly visible on open sea areas.

In the next step, various textural parameters have been calculated for VV and VH polarizations of Sentinel-1 images. From the list of available Grey Level Co-occurrence Matrix (GLCM) parameters [9], six features have been selected: Contrast, Dissimilarity, Entropy, Mean, Variance and Correlation. Other GLCM features are highly correlated with the selected ones and were excluded from the presented study.

The second group of features was composed of Hölder exponents determined by using four capacity measures – ABD, CAD, ISO and MSD, as described in [10, 11]. For the benchmark of ice detection performance with various features sets, 8 different scenarios were applied – Table 2.

Table 2. List of benchmark scenarios.

Scenario	Features	Number of features
1	VV + VH	2
2	VV + VH + 2 × ABD	4
3	VV + VH + 2 × CAD	4
4	VV + VH + 2 × ISO	4
5	VV + VH + 2 × MSD	4
6	VV + VH + 8 multifractal (2 × ABD, 2 × CAD, 2 × ISO, 2 × MSD) features	10
7	VV + VH + 12 GLCM (2×Contrast, 2×Dissimilarity, 2×Entropy, 2×Mean, 2×Variance, 2×Correlation)	14
8	VV + VH + 12 GLCM features + 8 multifractal features	22

Each textural feature has been calculated for both, VV and VH polarizations. For example, in Table 2, in the scenario 5, in total, four features have been used: VV, VH, MSD calculated on VV and MSD calculated on VH layer. Moreover, different sizes of calculation window were tested (5×5, 7×7 and 9×9).

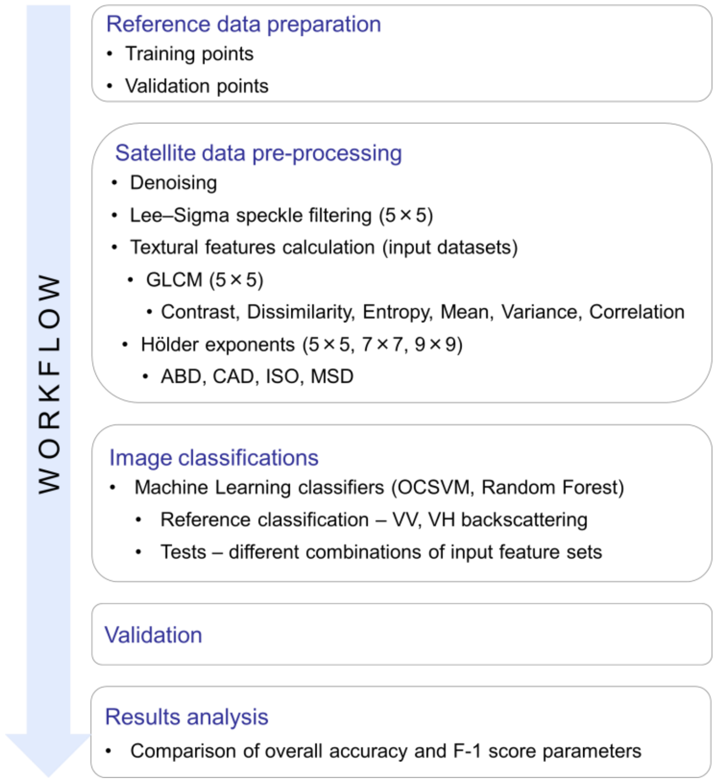

Figure 3. The general workflow of the experiment.

In the third stage, two different classification approaches have been applied. In the first one, only one class is used for training of the algorithm; in this case it was the information about ice. For this purpose, the state-of-the-art one class algorithm has been applied: OCSVM (One Class Support Vector Machine) [12]. In the second approach, the state-of-the-art multi-class classifier – Random Forest classifier [13] has been used with information about two classes: ice and water. Land area was masked out and was not classified within these experiments. Both classifiers can be tuned by the adjustment of specific parameters. For OCSVM, Gaussian radial basis function (RBF) kernel has been used and two parameters were optimized using the grid search approach and the accuracy board (Figure 5), proposed in [13]. For both classifiers, firstly, the tuning of parameters was performed. OCSVM was applied 150 times for each of 8 scenarios. In this way, the classifications have been performed with various combinations of: *γ (gamma)* – a RBF kernel width and *ν (nu)* parameters The value of ν indicates the assumed fraction of outliers within the training dataset. The full list of tested parameters values is presented in Table 3. In case of Random Forest, the number of the decision trees in algorithm was defined as 100.

Table 3. List of tested parameters values used in the grid search to find the best combination for OCSVM.

Parameter	**Values**
gamma (γ)	2^{-4}, 2^{-3}, 2^{-2}, 2^{-1}, 2^{0}, 2^{1}, 2^{2}, 2^{3}, 2^{4}, 2^{5}, 2^{6}, 2^{7}, 2^{8}, 2^{9},2^{10}
nu (ν)	0.01, 0.1, 0.2, 0.3, 0.4, 0.5, 0.6, 0.7, 0.8, 0.9

The full reference training dataset contains the 250 reference points. 187 represents the ice sample points, 63 – water. The imbalance between the amounts of training points was related to the fact that there are various different types of ice. In such way, within the training samples of ice, all of the ice types should be included.

Reference dataset used for quality assessment of ice cover maps generated within each scenario (Table 2) included 250 randomly selected and manually classified samples. Reference dataset contains: 197 sample points of ice and 53 sample points of water. The imbalance between the amounts of validation points, by analogy to the class distribution in the training dataset was related to the fact that there are various different types of ice. To evaluate the accuracy of each scenario, error matrices were generated and accuracy parameters – Overall Accuracy (OA), Producer Accuracy (PA), User Accuracy (UA), F1-score – have been calculated and compared in the last step of the experiment.

5. RESULTS

The quality assessment was performed for the image acquired by Sentinel-1 on December 5th, 2019. Figure 4 presents the subset of Sentinel-1 image and the corresponding classification map of ice (red colour) and water (blue colour). The area of land was masked out (grey colour), as only sea surface was analysed within this experiment.

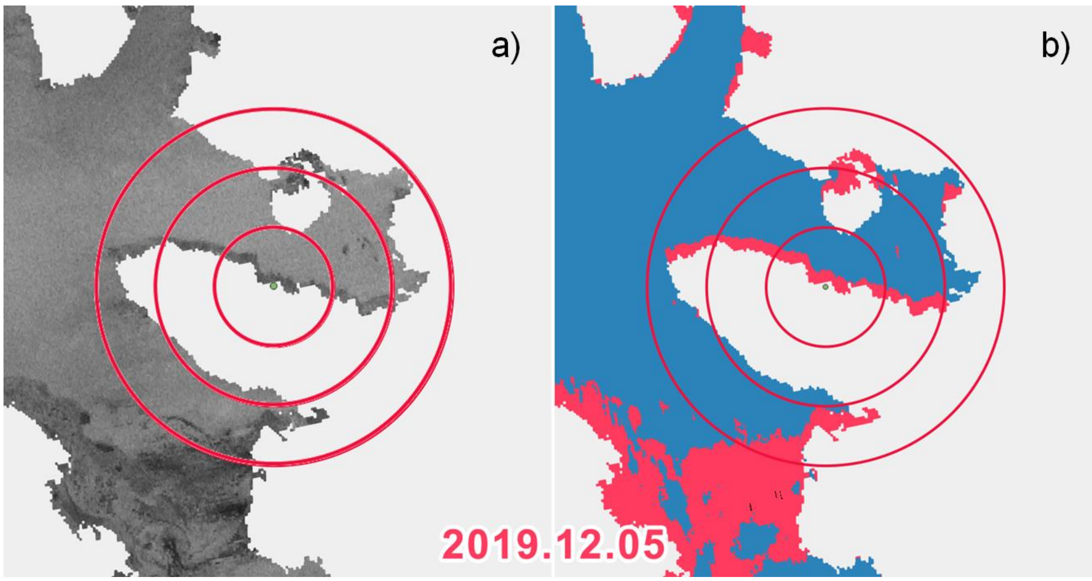

Figure 4. Sea ice extent on December 5th, 2019: a) subset of Sentinel-1 satellite image, b) subset of classification result (blue – water, red – sea-ice). Grey colour represents land. Red circles indicate the buffer around research station with radius of 5, 10 and 15 km. Result of Random Forest classifier.

Regarding OCSVM classifier, the best OA values, among 150 classifications, were used for selection of the optimal algorithm parameters. In most cases the highest OA and the highest F1-score value of ice was achieved for the same pair of parameters. The best values of *gamma* and *nu* parameters are 8 and 0.01 for reference dataset (scenario 1). However, the best fitted parameters values vary depending on scenario. The optimal parameters pairs for certain scenarios are presented in Table 4. Low values of *nu* indicate the high homogeneity of reference dataset, so it correctly represents the variability within the ice class. If *nu* value is 0.01, it means that only 1% of training samples was treated as outliners by the classifier (~2 points from 187). If *nu* value is 0. 1, it means that 10% of training points is treated as outliers (~20 points from 187). Example of accuracy board which is used to identify the best OCSVM parameters is presented in Figure 5.

Table 4. Optimal values of OCSVM parameters for analysed scenarios.

Scenario	1	2	3	4	5	6	7	8
gamma (γ)	2^3	2^2	2^2	2^3	2^2	2^0	2^0	2^0
nu (v)	0.01	0.1	0.1	0.1	0.1	0.01	0.1	0.2

The values of the Overall Accuracy achieved in 8 experimental scenarios, are presented in the left panels of: Figure 6 for OCSVM and Figure 7 for Random Forest classifier. Here, the red colour indicates the OA value from the first scenario, where only VV and VH backscattering values were used as the feature set. This scenario is used as a reference one.

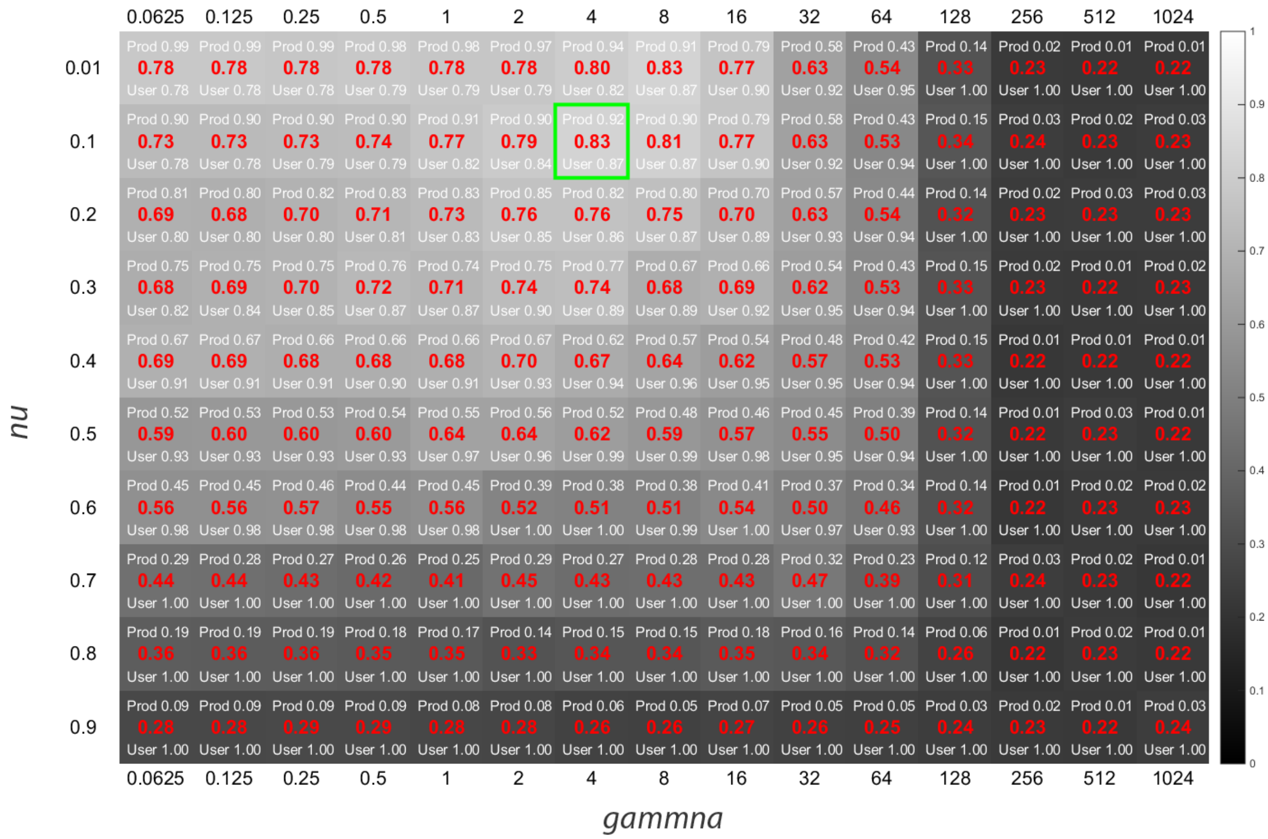

Figure 5. Example of the accuracy board, calculated for scenario 2, with OCSVM classifier. Red value: F1-score of ice class, White values: Producer and User Accuracy of ice detection. Green frame: the highest F1- score within this scenario.

Comparison of scenarios 2-8 to the scenario 1 indicates which textural features may improve the sea ice detection. Figure 6 (right panel) and Figure 7 (right panel) present the complex diagram, where F1-score values of two classes – ice (solid line) and water (dotted line), are compared. In this case, the reference scenario (1) is in red, while the other 7 scenarios results – in blue colour. On both plots, the results relate to the calculation window size 5×5.

In case of OCSVM, the OA of reference dataset was 83%. The same of OA was achieved only in the scenario 2, where additionally to the backscattering features, the ABD Selected Hölder features were used. Analysing the F1-score, we can observe that the accuracy of ice detection is very stable in all scenarios. On the other hands, F1-score for water class is significantly lower, comparing to the ice class. It is caused by the fact that this particular classifier, OCSVM, did not use any information about sea class in the training dataset. As the main goal of this study is ice detection, in case of OCSVM, values of water detection metrics should be used only as a complementary information. In four cases (scenarios 2, 4, 7 and 8) adding textural features resulted in improvement of F1-score values of water. Adding other combination of feature sets decreased the value of F1-score for water.

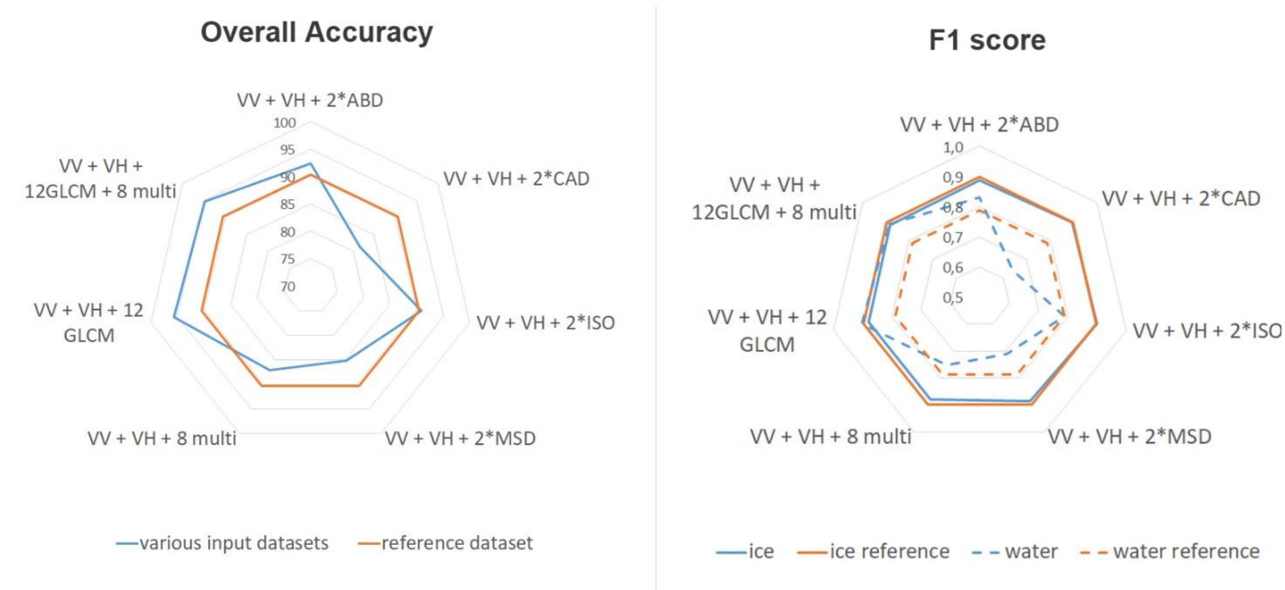

Figure 6. Overall accuracy (OA) and F1 score of various classification inputs, for OCSVM classifier and 5×5 calculation window size.

Using Random Forest algorithm, the reference datasets resulted in 90.4% of overall accuracy, F1-score for ice – 0.90 and for water – 0.83. Tests with higher number of the decision tree indicated that 100, that the increase of tree number improves the classification accuracy by 2%. Adding textural features may improve the accuracy of classification (OA) by 4-5%. Selected Hölder exponents resulted in the increase of OA, specifically ABD and ISO; by 0.5-2%. Adding two other Hölder exponents resulted in decrease of OA – CAD and MSD by 3-9%. Moreover, the calculation window size influences the accuracy of classification based on Hölder exponents. More precisely, in the case of the using 8 Hölder exponents determined in 5×5 window size, OA is 87.15%, using 9×9 – 91.20%. In general, in all tested feature sets, F1-score of ice is stable. F1-score of water increases in 3 cases: if we add 12 GLCM features (11%), 12 GLCM and 8 Hölder exponents (10%), or of solely ABD (4%). Adding CAD or MSD features decreases F1-score of water by 15% and 8%, respectively.

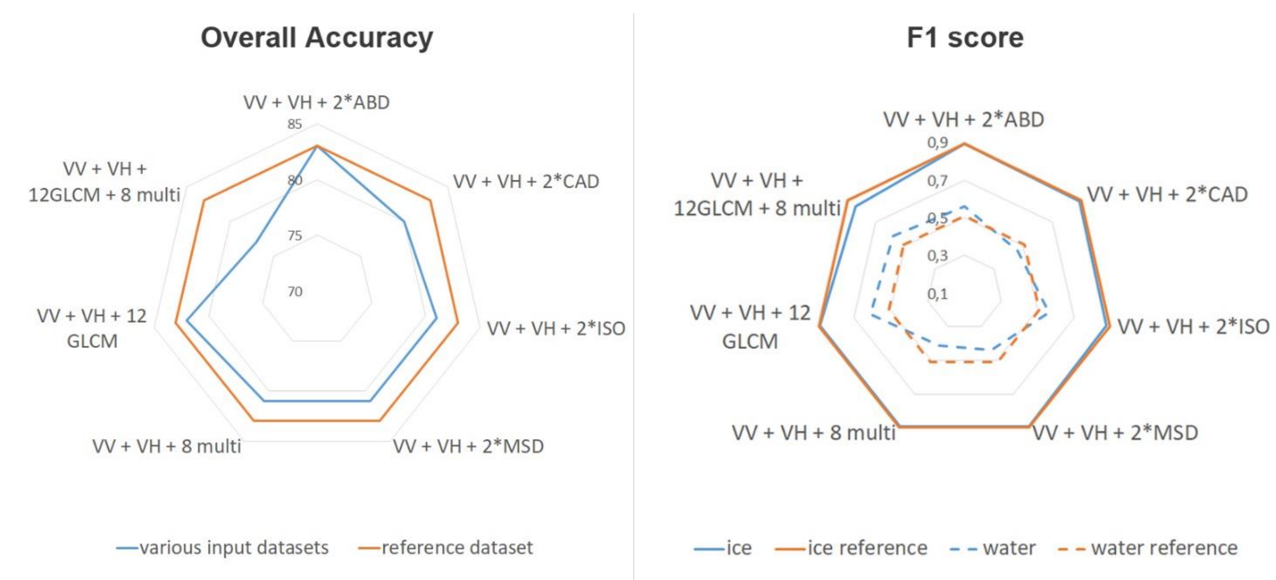

Figure 7. Overall accuracy (OA) and F1 score of various classification inputs, for Random Forest classifier and 5×5 calculation window size.

6. CONCLUSIONS AND DISCUSSION

The goal of the experiment was to develop the classification approach for high resolution ice mapping with Sentinel-1 images. For this purpose, we evaluated the influence of incorporation of various textural features (GLCM and Hölder exponents) into the sea ice mapping process. Comparison of eight different scenarios, using accuracy measures indicated the following main conclusions:

- adding textural features improves the classification accuracy, especially when Random Forest classifier is applied;
- higher classification accuracy was obtained with Random Forest, then OCSVM classifier;
- Hölder exponents may increase or decrease the accuracy of classification;
- in the case of Hölder exponents parameters, usage of bigger window size is recommended to enhance the classification performance;
- to provide more detailed information on how different feature sets influence the classification accuracy, various types of sea-ice should be investigated.

In the future, the extension of presented experiment is foreseen, by introduction of different types of ice identification.

7. ACKNOWLEDGEMENTS

This work was supported by the European Union's Horizon 2020 research and innovation programme under EOTIST project, grant agreement No 952111. AB and AP acknowledge funding by EU - Next Generation EU Mission 4 "Education and Research" - Component 2: "From research to business" - Investment 3.1: "Fund for the realisation of an integrated system of research and innovation infrastructures" - Project IR0000032 – ITINERIS - Italian Integrated Environmental Research Infrastructures System - CUP B53C22002150006.

REFERENCES

[1] Park, J.-W., Andreevich Korosov, A., Babiker, M., Won, J.-S., Wergeland Hansen, M., and Kim, H.-C., "Classification of sea ice types in Sentinel-1 synthetic aperture radar images", *The Cryosphere*, vol. 14, no. 8, pp. 2629–2645, 2020. doi:10.5194/tc-14-2629-2020.

[2] DiGirolamo, N., C. L. Parkinson, D. J. Cavalieri, P. Gloersen, and H. J. Zwally. (2022). Sea Ice Concentrations from Nimbus-7 SMMR and DMSP SSM/I-SSMIS Passive Microwave Data, Version 2 [Data Set]. Boulder, Colorado USA. NASA National Snow and Ice Data Center Distributed Active Archive Center. https://doi.org/10.5067/MPYG15WAA4WX. Date Accessed 08-12-2023.

[3] Meier, W. N., J. S. Stewart, H. Wilcox, M. A. Hardman, and D. J. Scott. (2021). Near-Real-Time DMSP SSMIS Daily Polar Gridded Sea Ice Concentrations, Version 2 [Data Set]. Boulder, Colorado USA. NASA National Snow and Ice Data Center Distributed Active Archive Center. https://doi.org/10.5067/YTTHO2FJQ97K. Date Accessed 08-12-2023.

[4] Spreen, G., L. Kaleschke, and G.Heygster (2008), Sea ice remote sensing using AMSR-E 89 GHz channels J. Geophys. Res.,vol. 113, C02S03, doi:10.1029/2005JC003384.

[5] Ludwig, V., G. Spreen, & L. T. Pedersen (2020). Evaluation of a New Merged Sea-Ice Concentration Dataset at 1 km Resolution from Thermal Infrared and Passive Microwave Satellite Data in the Arctic. Remote Sens. 12(19), 3183. doi:10.3390/rs12193183

[6] U.S. National Ice Center. 2020, updated daily. U.S. National Ice Center Daily Marginal Ice Zone Products, Version 1. [Indicate subset used]. Boulder, Colorado USA. NSIDC: National Snow and Ice. Data Center. https://doi.org/10.7265/ggcq-1m67.

[7] Norwegian Ice Service charts: https://cryo.met.no/en/latest-ice-charts

[8] Park, J.-W., Korosov, A. A., Babiker, M., Sandven, S., and Won, J.-S.: Efficient thermal noise removal for Sentinel-1 TOPSAR cross-polarization channel, IEEE T. Geosci. Remote, 56, 1555–1565, https://doi.org/10.1109/TGRS.2017.2765248, 2018.

[9] Haralick, R., "Statistical and Structural Approaches to Texture", IEEE Procedings, 67(5), 786-804 (1979).

[10] T. Stoji´c, I. Reljin, and B. Reljin, “Adaptation of multifractal analysis to segmentation of microcalcifications in digital mammograms,” Phys. A, Stat. Mech. Appl., vol. 367, pp. 494–508, Jul. 2006, doi:10.1016/j.physa.2005.11.030
[11] S. Aleksandrowicz, A. Wawrzaszek, W. Drzewiecki, M. Krupiński and M. Jenerowicz, "Change Detection in Multispectral VHR Images Using Spatialized Hölder Exponent," in IEEE Geoscience and Remote Sensing Letters, vol. 19, pp. 1-5, 2022, Art no. 5000705, doi: 10.1109/LGRS.2021.3060837.
[12] Chih-Chung Chang and Chih-Jen Lin, LIBSVM : a library for support vector machines. ACM Transactions on Intelligent Systems and Technology, 2:27:1--27:27, 2011. Software available at http://www.csie.ntu.edu.tw/~cjlin/libsvm
[13] Breiman, L. Random Forests. Mach. Learn. 2001, 45, 5–32.
[14] M. Krupiński, S. Lewiński, R. Malinowski, "One class SVM for building detection on Sentinel-2 images," Proc. SPIE 11176, Photonics Applications in Astronomy, Communications, Industry, and High-Energy Physics Experiments 2019, 1117635 (6 November 2019); https://doi.org/10.1117/12.2535547